

Nanofluid flow and heat transfer from heated square cylinder in the presence of upstream rectangular cylinder under Couette-Poiseuille flow

Swati Sharma¹, Dilip K. Maiti^{*2}, Md. Mahbub Alam³ and Bhupendra K. Sharma¹

¹Department of Mathematics, Birla Institute of Technology and Science, Pilani - 333031 RJ, India

²Department of Applied Mathematics with Oceanology and Computer Programming,
Vidyasagar University, Midnapur-721102, WB, India

³Institute for Turbulence-Noise-Vibration Interaction and Control,
Harbin Institute of Technology (Shenzhen), Shenzhen 518055, China

(Received September 7, 2018, Revised February 26, 2019, Accepted February 28, 2019)

Abstract. A heated square cylinder (with height A^*) is kept parallel to the cold wall at a fixed gap height $0.5A^*$ from the wall. Another adiabatic rectangular cylinder (of same height A^* and width $0.5A^*$) is placed upstream in an inline tandem arrangement. The spacing between the two cylinders is fixed at $3.0A^*$. The inlet flow is taken as Couette-Poiseuille flow based non-linear velocity profile. The conventional fluid (also known as base fluid) is chosen as water (W) whereas the nanoparticle material is selected as Al_2O_3 . Numerical simulations are performed by using SIMPLE algorithm based Finite Volume approach with staggered grid arrangement. The dependencies of hydrodynamic and heat transfer characteristics of the cylinder on non-dimensional parameters governing the nanofluids and the fluid flow are explored here. A critical discussion is made on the mechanism of improvement/reduction (due to the presence of the upstream cylinder) of heat transfer and drag coefficient, in comparison to those of an isolated cylinder. It is observed that the heat transfer increases with the increase in the non-linearity in the incident velocity profile at the inlet. For the present range studied, particle concentration has a negligible effect on heat transfer.

Keywords: tandem arrangement; heated cylinder; pressure gradient; Couette-Poiseuille flow; FVM

1. Introduction

The study of fluid flow and heat transfer around multiple bluff bodies has become a subject of considerable importance in recent years (e.g., Alam *et al.* 2002, Kim *et al.* 2016, Maiti *et al.* 2016, Bhatt *et al.* 2018, Sharma *et al.* 2018, Zafar and Alam 2018) because of its extensive applications in various industrial fields, such as cooling of glass, electronic equipment, drying of different materials and so on. It is important to understand the flow and its control over bluff bodies so that engineering design and public comfort can be improved continuously (e.g., Alam *et al.* 2003, 2006, 2010, 2018, Kim *et al.* 2018). Various studies have been carried out numerically as well as experimentally related to heat transfer characteristics of flow past bluff bodies. When the flow passes over multiple cylinders, a complex flow structure originates as a consequence of the mutual interactions among them. The wake structure forming behind the obstacles strongly depends on the shape and arrangement of the bodies and on the incoming flow. The flow becomes even more complicated when the wakes are further influenced by heat transfer and/or loading of nanoparticles in the base fluid.

Flow and heat transfer characteristics of a rectangular cylinder exposed to a uniform flow with ground effect have been studied by Shuja *et al.* (2001). Yang and Fu (2001)

studied the unsteady heat transfer from a heated electronic component subjected to a flow. Wang and Jaluria (2002) found that the heat transfer rate from a heated block increases with the height for fixed width, and decreases with increasing the width when the height is fixed. Maiti and Bhatt (2015) investigated the effect of pressure gradient at the inlet and observed that the steady flow converts to a periodic flow with the increase in the pressure gradient.

Devarakonda and Humphrey (1992) did an extensive study of the unsteady flow past a pair of square cylinders in tandem arrangement through an experimental-numerical approach. They concluded that the presence of the eddy promoter enhances the heat transfer from the downstream cylinder. A similar study was done by Tatsutani *et al.* (1993) for cylinder diameter ratio 2 (based on the upstream cylinder diameter) in which the smaller cylinder was placed at an optimal location, upstream of the large heated cylinder, which resulted in a maximum heat transfer from the downstream cylinder. Sohankar and Etminan (2009) numerically studied the heat transfer from tandem square cylinders and observed that the Nusselt number is larger for the upstream cylinder. Etminan *et al.* (2011) numerically studied the unconfined flow characteristics around the tandem square cylinders in both steady and unsteady laminar flow regimes at a fixed spacing, i.e., $S = 5$. Chatterjee and Mondal (2012) reported the effect of the spacing between the cylinders on heat transfer enhancement at different Reynolds numbers.

It is equally important to note that the heat transfer can be enhanced by the loading of nanoparticles in the base

*Corresponding author, Professor
E-mail: d_iitkgp@yahoo.com

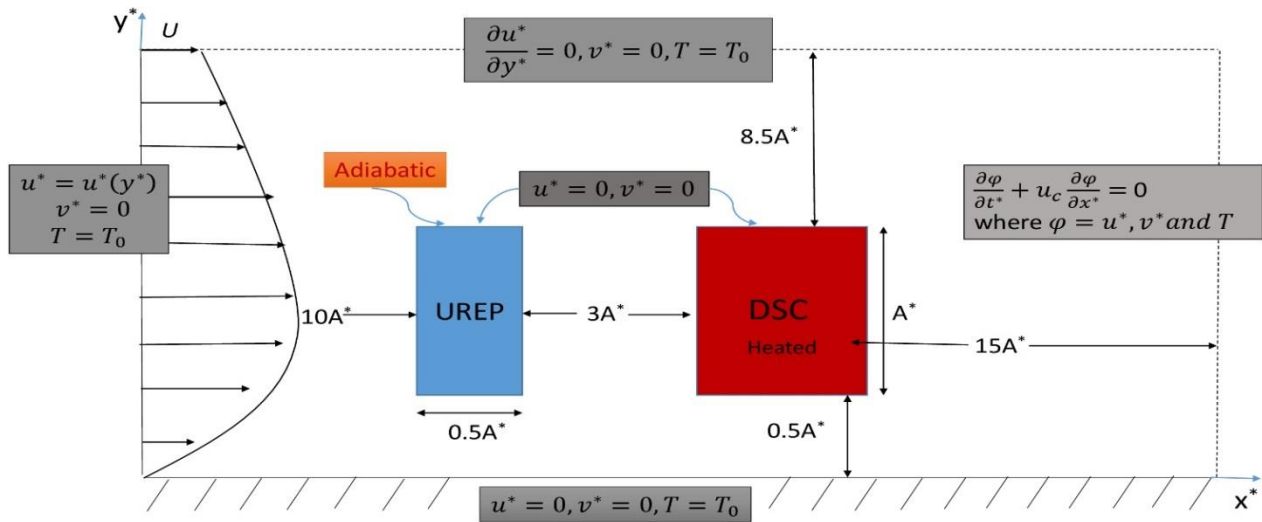


Fig. 1 Schematics of flow configuration (DSC referred to as the downstream square cylinder, and UREP as the upstream rectangular eddy promoter)

fluid. It was Choi (1995) who first used nanoscale particle suspensions (nanofluids) as an alternative heat transfer medium due to its superior thermal properties, improved stability, and homogeneity. The very small size of the nanoparticles (1–100 nm) imparts some unique physical and chemical properties to these nanofluids, as mentioned in the studies of Lee *et al.* (1999) and Eastman *et al.* (2004). Several numerical studies on convective laminar heat transfer using nanofluids as working fluid are reported in the literature. The fundamental studies on convective transport of nanofluids are rapidly increasing for engineering applications such as automotive sector, nuclear reactors, cooling of electronics and X-rays (Nguyen *et al.* 2007, Escher *et al.* 2011, Ahmed *et al.* 2012, Sarkar *et al.* 2016).

Hwang *et al.* (2007) reported that the solution (water-based Al_2O_3 nanofluids) is more stable than the base fluid. Sarkar *et al.* (2013) presented the global stability of nanofluids in a mixed convective flow at the onset of vortex shedding. For the unconfined flow of nanofluids over a square cylinder, Etminan *et al.* (2012) reported that there is an optimum value of ϕ that results in the highest heat transfer coefficient. Based on water-based nanofluids (using Cu and Al_2O_3), Sarkar *et al.* (2012) studied heat transfer characteristics past a circular cylinder in cross flow and observed that the presence of nanoparticles imparts a counterbalancing force to that of buoyancy force. For the case of square cylinders, Sarkar *et al.* (2013) observed that Cu-water and Al_2O_3 – water nanofluids show suppression of vortex shedding at Richardson number $Ri \geq 0.15$. Vortex shedding initiates and a completely new phenomenon comes into being when ϕ is increased.

Valipour *et al.* (2011) indicated that, at a given Reynolds number Re , local time-mean Nusselt number \overline{Nu} were enhanced by adding nanoparticles to the base fluid. Talebi *et al.* (2010) found, that, for any given Re and Rayleigh

number Ra , heat transfer in the enclosure, filled with Cu-water nanofluid with a moving top wall, increases with the volumetric fraction of the copper nanoparticles in the water.

Rayleigh-Benard problem was examined by Haddad *et al.* (2012) in which they observed that an enhancement in heat transfer is more pronounced at low volume fraction of nanoparticles under the effect of Brownian motion and thermophoresis for Cu-water nanofluid. Sarkar and Ganguly (2012) demonstrated the entropy generation due to laminar mixed convection of water-based nanofluid (using Cu, Al_2O_3) past a square cylinder in vertically upward flow with the range of ϕ : 0–20%. Sharma *et al.* (2018) numerically investigated the effect of concentration (ϕ), particle size (d_{np}) and pecllet number (Pe) on heat transfer from a long heated square cylinder placed near a cold wall under the incident of a Couette flow and observe that the Nusselt number is an increasing function of ϕ and Pe while it decreases with the increase of d_{np} .

From the above review, it is obvious that investigations on heat transfer from a cylinder neighbored by another in a flow with nanofluids are scarce. To the best of our knowledge, not a single article is available based on heat transfer around a square heated cylinder in the presence of another upstream rectangular cylinder near a wall under the incident of nonlinear velocity profile utilizing nanofluids. The objective of this work is to investigate the role of the nondimensional pressure gradient (P) at the inlet and of the nanofluid particle concentrations (ϕ) on the hydrodynamic and heat transfer characteristics of the heated cylinder. An effort is made to examine the mechanism of improvement/reduction of drag coefficient of and heat transfer from the heated cylinder in the presence of the upstream cylinder. There are some experimental works on heat transfer enhancement using nanofluids (e.g., Yang *et al.* 2005). Nonlinear velocity profiles are very common in channel flow with different pressure gradients.

2. Methodology

2.1 Problem formulation and governing equations

Fig. 1 shows the geometrical configuration along with the boundary conditions. Two cylinders of same height A^* are placed parallel to the wall at a fixed gap height of $0.5A^*$ from the wall. The distance between the two cylinders is fixed at $3A^*$. The cylinder at the downstream side (referred to as DSC) is of square cross-section whereas the upstream cylinder (referred to as UREP) is rectangular with its width being half of the square cylinder. The upstream flow field is taken as Couette-Poiseuille flow based non-linear velocity profile $u^* = \frac{y^*}{H^*}U + PU\frac{y^*}{H^*}\left(1 - \frac{y^*}{H^*}\right)$

where $P = \frac{H^{*2}}{2\mu_f U}\left(-\frac{dp^*}{dx^*}\right) = \frac{1}{2}H^2 Re \frac{\rho_{nf}}{\rho_f}\left(-\frac{dp}{dx}\right)$ is the non-dimensional pressure gradient, U is the velocity of the top plane wall at a gap height $10A^*$, $Re = \frac{UA^*}{\nu_f}$ is the Reynolds number, ρ , μ , and ν , stand for density, absolute viscosity, and kinematic viscosity, respectively. The subscript 'nf' and 'f' denote the nanofluid and base fluid respectively.

Detailed discussion on consideration of Couette-Poiseuille flow can be found in a study of Maiti and Bhatt (2015). The DSC is maintained at a constant temperature T_w , while the UREP is considered as an adiabatic. The wall and ambient stream are considered to be at T_0 with $T_0 < T_w$. Parameters governing the fluid flow are P at the inlet and Re . The flow is considered as two dimensional and laminar while the fluid is taken as nanofluid.

To the best of authors' knowledge, almost all the available studies on nanofluid flow over circular/triangular/square type bodies are based on a single-phase modeling approach, and therefore it is adopted here. The Navier-Stokes equations along with the energy equation governing the nanofluid flow and heat transfer characteristics are given by

$$\frac{\partial u}{\partial x} + \frac{\partial v}{\partial y} = 0 \quad (1)$$

$$\frac{\partial u}{\partial t} + \frac{\partial u^2}{\partial x} + \frac{\partial uv}{\partial y} = -\frac{\partial p}{\partial x} + \frac{1}{Re} * \frac{\partial_{nf}}{\partial_f} * \left(\frac{\partial^2 u}{\partial x^2} + \frac{\partial^2 u}{\partial y^2}\right) \quad (2)$$

$$\frac{\partial v}{\partial t} + \frac{\partial uv}{\partial x} + \frac{\partial v^2}{\partial y} = -\frac{\partial p}{\partial x} + \frac{1}{Re} * \frac{\partial_{nf}}{\partial_f} * \left(\frac{\partial^2 v}{\partial x^2} + \frac{\partial^2 v}{\partial y^2}\right) \quad (3)$$

$$\frac{\partial \theta}{\partial t} + \frac{\partial u\theta}{\partial x} + \frac{\partial v\theta}{\partial y} = \frac{1}{Re * Pr} * \frac{\alpha_{nf}}{\alpha_f} * \left(\frac{\partial^2 \theta}{\partial x^2} + \frac{\partial^2 \theta}{\partial y^2}\right) \quad (4)$$

Here u and v denote the non-dimensional velocity vector along the x - and y -direction, respectively, t is the time, and α is the thermal diffusivity. The governing equations are non-dimensionalised by A^* , U and $\rho_{nf}U^2$. Prandtl number (Pr) and non-dimensional temperature (θ) are respectively defined as $Pr = \frac{\nu_f}{\alpha_f}$ and $\theta = \frac{T-T_0}{T_w-T_0}$.

2.2 Nanofluid model

Density, effective viscosity, Specific heat, and thermal conductivity of nanofluids are calculated from relations available in Etminan *et al.* (2012). Nanofluid modeling, temperature of the base fluid, mean nanoparticle diameter, nanoparticle volume fraction, nanoparticle density, and base fluid physical properties are considered here. The detailed discussion on the calculation of the thermophysical properties of nanofluids, like density, specific heat, thermal conductivity and viscosity can be found in our previous study (Sharma *et al.* 2018). Nanofluid is considered as $W - Al_2O_3$. Parameters governing the nanofluid is particle concentrations (ϕ).

2.3 Definitions of hydrodynamic and heat transfer characteristics

The coefficients of the time-mean drag (C_D) and lift (C_L) on the cylinder are calculated from the following expression

$$C_D = C_{DP} + C_{DSh} = \frac{F_D}{0.5\rho U^2 A^*} \quad (5)$$

$$C_L = C_{LP} + C_{LSh} = \frac{F_L}{0.5\rho U^2 A^*}$$

where C_{DP} and C_{DSh} represent the time-mean drag coefficients due to pressure and viscous forces, respectively; similarly, C_{LP} and C_{LSh} represent the lift coefficient due to pressure and viscous forces, respectively, F_D and F_L are the time-mean integrated drag and lift forces acting on the cylinder, respectively.

The local Nusselt number (Nu), face-wise average Nusselt number (Nu_{avg}), local time-averaged Nusselt number (\overline{Nu}), face-wise time-averaged Nusselt number (\overline{Nu}_{avg}), and time- and surface-averaged Nusselt number (\overline{Nu}_M) of the cylinder are defined, respectively, as

$$Nu = \frac{hA^*}{k_{nf}}, Nu_{avg} = \frac{1}{A^*} \int_0^{A^*} (Nu) dl \text{ along a face, } \overline{Nu} = \frac{1}{\sum_t} \sum_t t Nu(t) \text{ at each point on faces,}$$

$$\overline{Nu}_{avg} = \frac{1}{A^*} \int_0^{A^*} (\overline{Nu}) dl \text{ along a face and } \overline{Nu}_M = \frac{1}{4} \sum_{\text{faces}} \overline{Nu}_{avg}$$

where h and k_{nf} are convective heat transfer coefficient and thermal conductivity of nanofluid, respectively.

2.5 Numerical method

The computational domain is divided into Cartesian cells. The pressure correction based iterative algorithm SIMPLE (Patanker 1980), based on the finite volume method (FVM) with staggered grids, is applied here. A third order accurate QUICK (Quadratic Upstream Interpolation for Convective Kinematics, Leonard (1976)) is employed to discretise the convective terms and central differencing for diffusion terms. A fully implicit third order scheme is incorporated to discretise the time derivatives. The pressure link between continuity and momentum is accomplished by transforming the continuity equation into a Poisson equation for pressure. The Poisson equation implements a

pressure correction for a divergent velocity field. A detailed discussion of the numerical methodology (staggered grid, FVM, QUICK and SIMPLE algorithms) used here has been made in the previous study (Bhattacharyya and Maiti 2004).

2.6 Validation of numerical code

The numerical code is already validated for the case of nanofluid modeling and single cylinder with Etminan *et al.* (2012) and presented in Table – 1 of our previous study (Sharma *et al.* (2018)). The numerical code for the cases of heat transfer around two equal isothermal square cylinders placed in a tandem arrangement is validated with Chatterjee and Mondal (2012) and Sohankar *et al.* (2009) for different values of Re and presented in Figs. 2 and 3. An excellent match between the two results in time- and surface-mean Nusselt number (\overline{Nu}_M) as well as drag coefficient (C_D) for both upstream and downstream cylinders are observed.

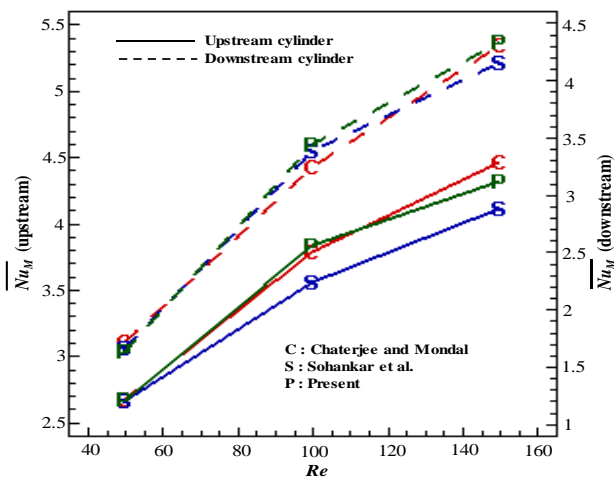


Fig. 2 Validations of present time- and surface-averaged Nusselt numbers with those of Chatterjee and Mondal (2012) (C) and Sohankar *et al.* (2009) (S) for $S = 5$

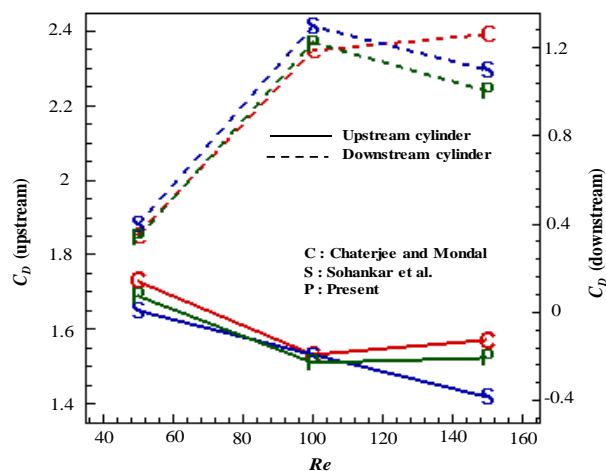


Fig. 3 Validation of present time-mean drag coefficients with those of Chatterjee and Mondal (2012) (C) and Sohankar *et al.* (2009) (S) for $S = 5$

3. Results and discussion

Numerical simulations are presently performed to examine the effects of particle concentration ϕ and pressure gradient P on hydrodynamic and heat transfer characteristics of the nanofluids. The P is varied as $0 \leq P \leq 5$ while ϕ is considered upto 5% (Sharma *et al.* 2018). The diameter of the nanoparticle d_{np} is fixed at 50 nm. The Re is kept constant at 250, and the value of Pr is taken as 6.14 for $W-Al_2O_3$ nanofluid. It may be noted that, due to variation in ϕ , only physical properties of nanofluid (ν_{nf} and α_{nf}) are changed, which are reflected in Eqs. (2)-(4).

To investigate the effect of nonlinearity of the inlet flow on the flow field, the instantaneous vorticity lines for $W-Al_2O_3$ nanofluid are shown in Fig. 4 (left side) at $\phi = 3\%$. As seen, the flow is completely steady up to $P = 4$, and no vortex shedding takes place behind the cylinder. Up to $P = 3$, the upper shear layer issuing from the UREP merges with its DSC counterpart and emerges horizontally in the streamwise direction, while the lower shear layer of the UREP reattaches with the front face of the DSC. At $P = 3$ and 4, the steady gap reattachment of the shear layers is found. Unsteadiness is generated in the flow at $P = 5$. Clearly, the upstream cylinder sheds vortices alternatively, and the shed negative vortices (black color) roll over the top of the downstream cylinder while the positive vortices impinge on the front face of DSC and then pass through the gap between the wall and the bottom face of the DSC. Therefore, the nanofluid flow over the downstream cylinder can be made unsteady by increasing P at a lower Re at which the isolated square cylinder flow was reported to be steady.

As both vorticity and thermal energy are being transported by the flow in the wake, contours of temperature are equivalent to those of vorticity. As can be seen from Fig. 4 (right side), the insulation layer (thermal boundary layer) around the cylinder surfaces, especially at the front, lower and upper surfaces, decreases with the increase of P . This is due to the fact that the incident velocity on the cylinder becomes stronger at a higher P . It is worth noting that the crowding of isotherms in the recirculation region (behind the rear face) increases with P , causing a noticeable change in the isotherm pattern. Therefore, by generating unsteadiness in the flow by increasing P , the heat transfer from the rear face of DSC is expected to improve.

Fig. 5 shows the time-averaged surface pressure \overline{C}_p distributions along the DSC's bottom face and the plane wall (see Fig. 5(a)) and time-averaged streamwise velocity (\overline{u}) profile along y (see Fig. 5(b)) at the exit position of the gap flow between the DSC's bottom face and the plane wall.

As can be seen, the pressure difference between the bottom face and the plane wall is almost zero at $P = 0$ and 3 in the core of the gap region. As a result, the gap flow becomes unidirectional, and the core flow looks like a channel flow, owing to the fact that the interaction between shear layers of the cylinder get lost. Therefore, the vortex shedding is completely suppressed at $P = 0$ and 3. On the other hand, at $P = 5$, the pressure on the bottom face is less

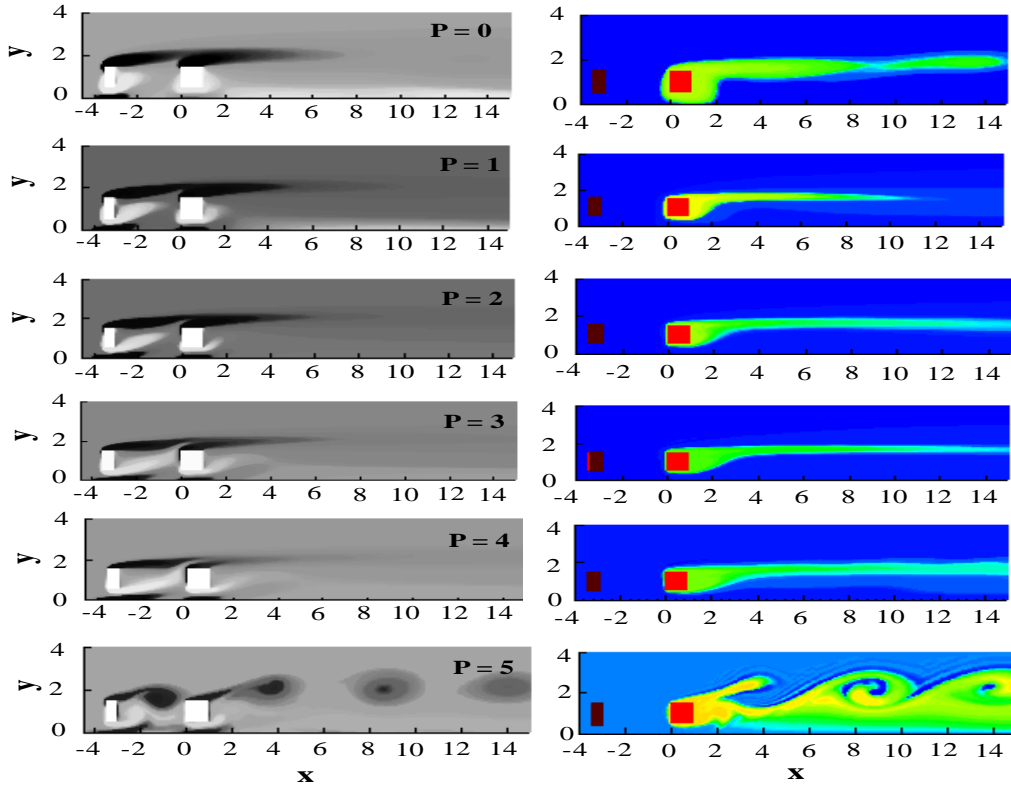


Fig. 4 Vorticity contours (left side) and corresponding isotherms (right side) at different P at a spacing $S = 3$, $Re = 250$ for $\phi = 3\%$

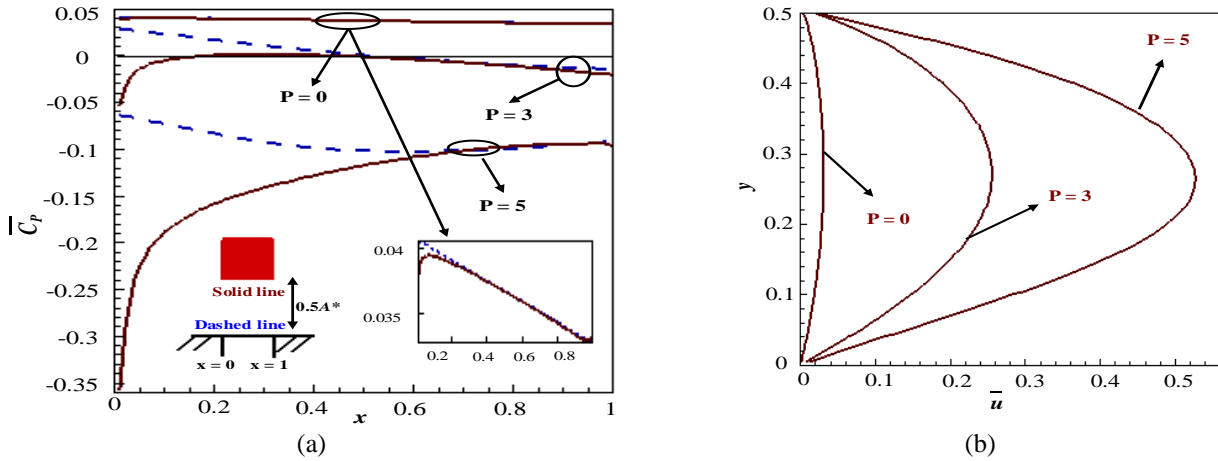


Fig. 5 (a) Surface pressure distribution ($\overline{C_p}$) along the plane wall (dashed line) and along the lower face of the downstream cylinder at $\phi = 3\%$ and (b) Time-mean streamwise velocity distributions along the y -direction at $x = 1$ between the DSC lower face and the plane wall for $\phi = 3\%$

than that on the wall. As a result, the interaction of DSC shear layers takes place in the wake, leading to the vortex shedding. It is evident from the Fig. 5(b) that the velocity profiles overshoot, and the gap flow (which plays a major role in the vortex shedding behind the cylinder) becomes stronger with the increase of P . Also, the position at which the maximum velocity occurs shifts closer to the wall at the highest value of $P = 5$. This confirms the existence of unsteadiness in the flow of DSC (Maiti 2012).

Unsteadiness in the wake of the DSC at $P = 5$ is reconfirmed with the help of phase (u vs v at a point $3A^*$ distance from the rear face of the DSC) diagram in Fig. 6. As seen in Fig. 6, a limit cycle exists at both $\phi = 0$ and 5% with $P = 5$, indicating the existence of periodic flow with a single, sharp peak in the spectra of fluctuating lift coefficient of the DSC (Fig. 6(b)). It is clear that concentration ϕ has a very negligible influence on the hydrodynamic characteristics in the considered range of ϕ here.

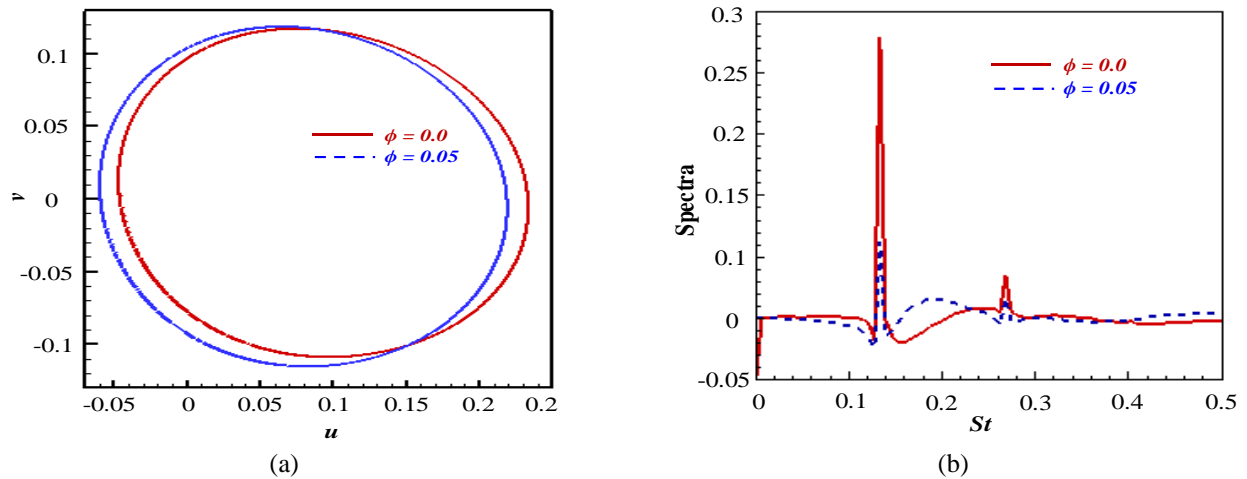


Fig. 6. (a) Phase diagram (u against v at a location of $3A^*$ from the rear face of the DSC), and (b) spectra of fluctuating lift coefficient of the DSC for $\phi = 0$ and 5% at $P = 5$

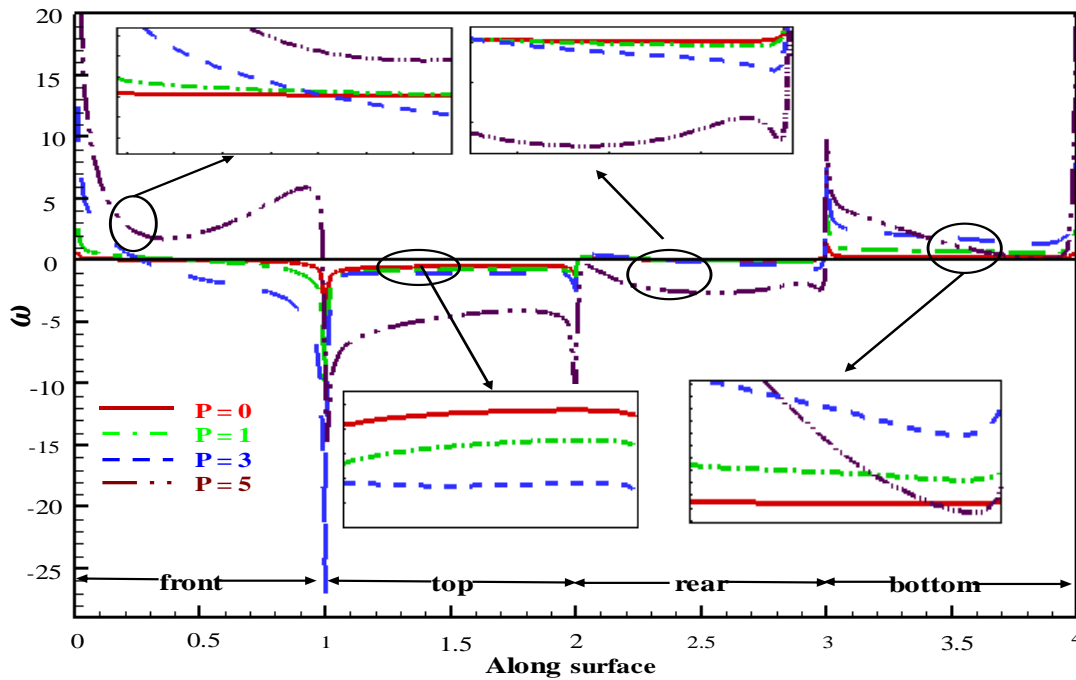


Fig. 7 Wall vorticity around surfaces of the DSC for different P with $\phi = 3\%$

The effect of nonlinearity (P) on the wall vorticity generated at the surfaces of the DSC is exemplified in Fig. 7 for $\phi = 3\%$. All the curves are qualitatively similar to each other. Overall, the sharpest variation in the wall vorticity ω can be seen at the front-top corner, pointing to a large variation in the velocity. The global minimum and maximum of ω register at points 1 and 0, respectively. The front stagnation point is largely affected by the variation of P . The curve for $P = 5$ distinctly appears in the figure. As seen, the magnitude of ω is directly proportional to P since the increase of P is equivalent to increase the intensity of the incidence velocity under the present flow condition.

Fig. 8 plots the time-averaged local Nusselt number (\overline{Nu}) distributions around the DSC surfaces for $P = 0, 1, 3$ & 5 at a fix $\phi = 3\%$. As seen from Fig. 8, \overline{Nu} attains a local maximum at all of the four corners, having a global maximum at the front top corner (point 1 in Fig. 8), because of the steepest temperature gradient. Apparently, \overline{Nu} at each point on the surface of the downstream cylinder is proportional to P . As a result, the total heat transfer from the cylinder is expected to be large as long as P is high. The front face (0-1 in Fig. 8) shows higher heat transfer among all other faces since the incoming cold fluid first contacts the outgoing hot fluid surrounding the hot cylinder.

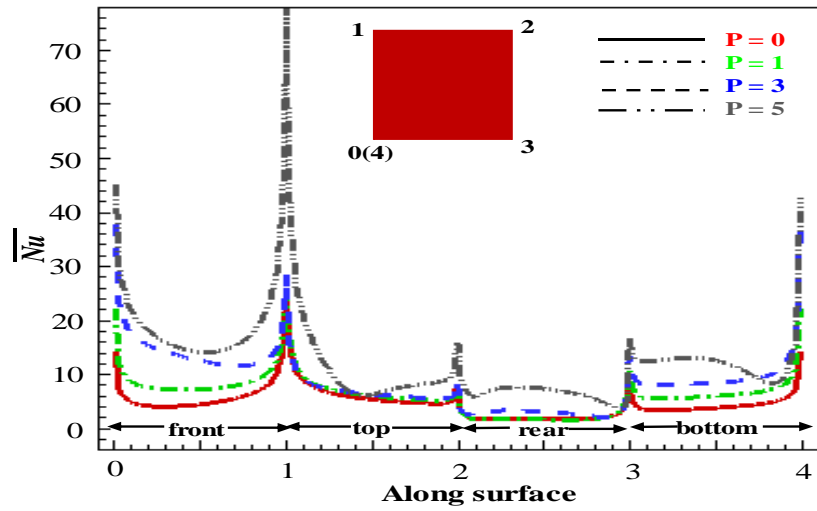


Fig. 8 Nusselt distributions along the surfaces of the DSC for different P with $\phi = 3\%$

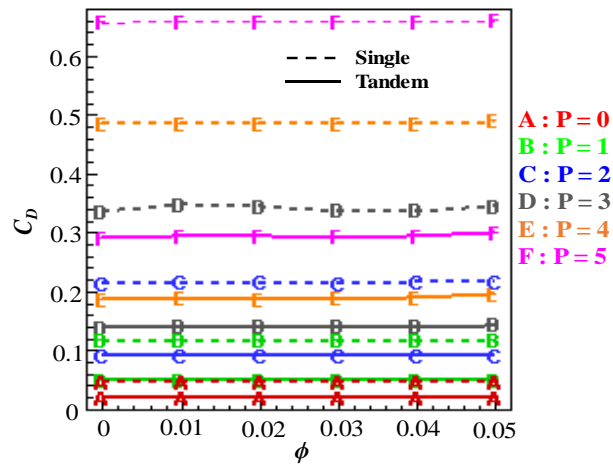


Fig. 9 Variation in C_D with ϕ at different P

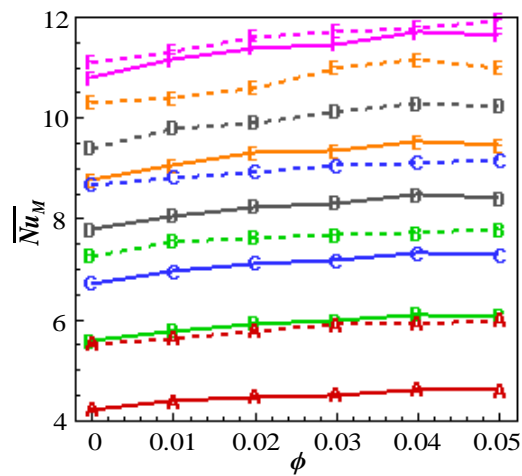
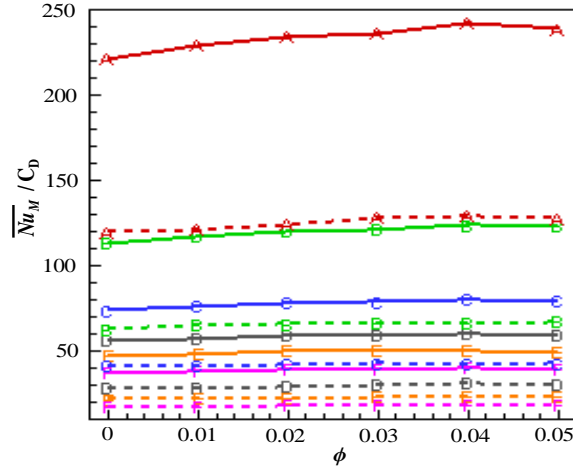


Fig. 10 Time-averaged mean Nusselt number of the DSC as a function of ϕ at different P

Table 1 Propose dependency of \overline{Nu}_M on ϕ and P in the functional form $\overline{Nu}_M = \overline{Nu}_M(P)$ and on $\overline{Nu}_M = \overline{Nu}_M(\phi)$

$\phi \downarrow$	$\overline{Nu}_M = \overline{Nu}_M(P)$	$P \downarrow$	$\overline{Nu}_M = \overline{Nu}_M(\phi)$
0.0	$4.2e^{0.00925P^3 - 0.0807P^2 + 0.3606P}$ (0.01482, 0.9994)	0	$-0.04504\phi^{3/2} + 0.1624\phi + 0.03635\phi^{1/2} + 4.221$ (0.001567, 0.9857)
0.03	$4.492e^{0.00924P^3 - 0.08086P^2 + 0.3605P}$ (0.01549, 0.9995)	3	$(-0.01181\phi^3 - 0.4130\phi^2 + 4.408\phi + 60.65)^{1/2}$ (0.005776, 0.9821)
0.05	$4.582e^{0.009414P^3 - 0.08143P^2 + 0.3581P}$ (0.01588, 0.9995)	5	$-0.01283\phi^{3/2} + 0.4462\phi + 0.04072\phi^{1/2} + 10.784$ (0.009836, 0.9831)

Fig. 11 Ratio of time-average mean Nusselt number to drag coefficient at different P and ϕ at $Re = 250$

The time-averaged drag coefficient as a function of ϕ is presented in Fig. 9 at different P . It can be easily noticeable that the time-mean drag coefficient C_D increases with increasing P but it is very weakly dependent on the nanoparticle concentration ϕ . It may be noted that the increase of Reynolds number is mechanically similar to the increase of P since $-\frac{dp}{dx} = 2P \left(\frac{1}{h}\right)^2 \left(\frac{1}{Re}\right)$ and is fixed.

Therefore the change in P will have much effect on the flow field, consequently on the hydrodynamic characteristics. Nominal increase in C_D due to ϕ is due to the fact that nanofluid viscosity increases with ϕ . Comparing the value of isolated square cylinder at respective P value, it is seen that the drag coefficient of the DSC declines due to sheltering effect by the UREP. The reduction is found more as long as P is high.

The effect of P on the time- and surface-averaged Nusselt number (\overline{Nu}_M) with different ϕ is presented in Fig. 10. As can be observed in Fig. 10, \overline{Nu}_M increases with increasing P and ϕ but the effect of non-linearity of incident velocity P is more pronounced than that of ϕ . The concentration influence on heat transfer is slightly more prominent at higher P . It is evident from Fig. 10 that \overline{Nu}_M of the DSC decreases at all P . This is physically realistic, because the \overline{Nu} values at the front face that is the major contributing face to the total \overline{Nu}_M is drastically reduced by the UREP (ref. Fig. 8). At a lower P , the exchange of ambient cold fluid and hot fluid near to the front face of the

DSC is found to be minimum, and with the increase of P , this exchange of fluids increases due to oscillatory behaviour of the shear layers of the UREP, indicating recovery of \overline{Nu} from the front face (ref. Fig. 4). Consequently the difference in \overline{Nu}_M between the isolated and tandem cases decreases with the increase in P .

The ratio $\frac{\overline{Nu}_M}{C_D}$ is presented in Fig. 11. It is observed from Figs. 9 and 10 that the heat transfer from the DSC is reduced by the UREP, while increasing with P and ϕ . At the same time, the drag coefficient of the DSC also reduces because of the sheltering effect by the UREP, while it increases with P and ϕ . Now, it is evident from Fig. 11 that their ratio $\frac{\overline{Nu}_M}{C_D}$ increases nominally with ϕ , however, decreases with P . The curve for $P = 0$ distinctly appears at the top, indicating that consideration of linear velocity profile at the inlet is beneficial in terms of heat transfer enhancement together with minimum drag coefficient from the DSC. It may be noted that the ratio is larger for nanofluid than for the clear fluid at all P , remarkably at lower P . At a particular ϕ , a drastic jump in $\frac{\overline{Nu}_M}{C_D}$ is observed when the incident velocity is changed from linear to first non-linear form. The $\frac{\overline{Nu}_M}{C_D}$ is greater for tandem case than for single cylinder, and the difference in $\frac{\overline{Nu}_M}{C_D}$ between the two cases is large at a lower P , remarkable at $P = 0$.

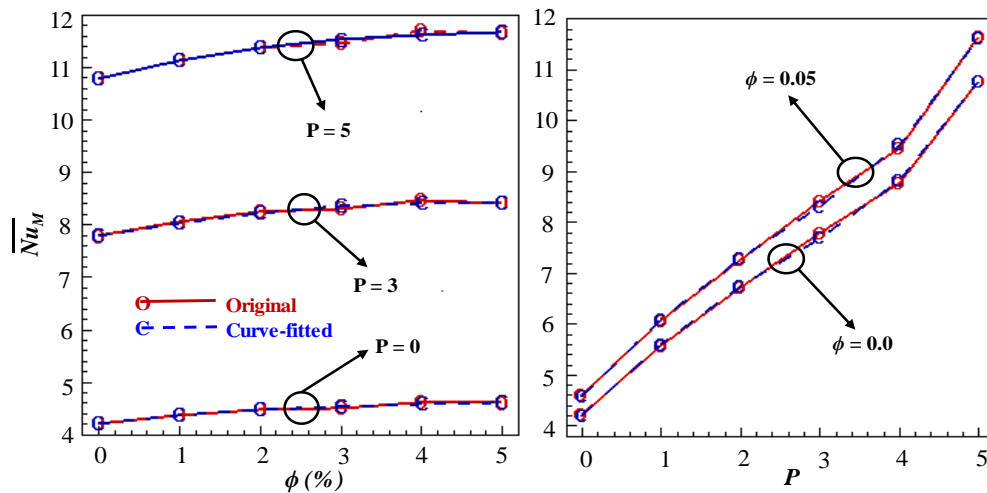


Fig. 12 Validation of proposed relations for (a) $\overline{Nu}_M = \overline{Nu}_M(\phi)$ and (b) $\overline{Nu}_M = \overline{Nu}_M(P)$ (as noted in Table 1) with that of original computed data

Table 1 shows the proposed relationship of \overline{Nu}_M on P and ϕ in the functional forms $\overline{Nu}_M = \overline{Nu}_M(P)$ and $\overline{Nu}_M = \overline{Nu}_M(\phi)$, respectively. These relations are fitted using the least square method based on the computed values for range of $\phi : 0 - 5\%$ and $P : 0 - 5$. Numerical values written in bracket against each relation are the residual sum of squares (RSS) and coefficient of determination (R^2). An R^2 of 0.99 means that it is 99% predictable. A small RSS indicates a tight fit of the model of the data. As can be seen from the table, all the values of R^2 lies in (0.9821, 0.9995) implies that the relations are best fitted.

In order to validate these relations, Fig. 12 is presented to compare the original computed values with the values obtained by proposed relations. It is evident from the figure that all the fitted values are well correlated with the original computed values and hence, one can predict the \overline{Nu}_M at different P and ϕ (within the considered range of P and ϕ) using these proposed relations.

4. Conclusions

The present study deals with the numerical investigation of nanofluid flow around a heated square cylinder in the presence of upstream rectangular cylinder placed at a gap height of $0.5A^*$ from the wall under the incidence of Couette- Poiseuille flow. The effects of pressure gradient P and nanoparticle concentration ϕ on the flow field and heat transfer characteristics are investigated. The numerically simulated results lead to the following conclusions.

- The shear layers issuing from the upstream cylinder merge with the shear layers of the downstream cylinder and form a steady closed circulation region between the cylinders at a lower P . At a higher P , the above recirculation region is opened and unsteadiness comes into being in the flow of the downstream cylinder at a lower Re at which isolated square cylinder reported to be steady.

- The heat exchange between ambient cold fluid and hot fluid near to the front face of the heated cylinder enhances with increasing P , as does the crowding of isotherms near the rear face of the downstream cylinder.
- The time- and surface-averaged heat transfer (\overline{Nu}_M) and drag coefficient (C_D) of the downstream cylinder are suppressed from those of an isolated situation due to the tandem effect. They however increase with increasing P and ϕ . Their ratio $\frac{\overline{Nu}_M}{C_D}$ increases nominally with ϕ , but decreases with the increase of P . A drastic jump in $\frac{\overline{Nu}_M}{C_D}$ is observed when P is changed from 0 to 1. The value of $\frac{\overline{Nu}_M}{C_D}$ is large for the tandem case than for the isolated case.
- The functional forms of $\overline{Nu}_M = \overline{Nu}_M(P)$ and $\overline{Nu}_M = \overline{Nu}_M(\phi)$ are proposed by the least square curve fitting method.

Acknowledgements

Maiti acknowledges the financial assistance of DST (INDIA) (Sanction No. SR/S4/MS/820/13 dated 07.05.2015).

References

- Ahmed, H.E., Mohammed, H.A. and Yusoff, M.Z. (2012), "An overview on heat transfer augmentation using vortex generators and nanofluids: approaches and applications", *Renew. Sust. Energ. Rev.*, **16**(8), 5951-5993. <https://doi.org/10.1016/j.rser.2012.06.003>.
- Alam, M.M., Moriya, M., Takai, K. and Sakamoto, H. (2002), "Suppression of fluid forces acting on two square prisms in tandem arrangement by passive control of flow", *J. Fluid. Struct.*, **16**(8), 1073-1092. <https://doi.org/10.1006/jfls.2002.0458>.
- Alam, M.M., Sakamoto H. and Zhou, Y. (2006), "Effect of a T-shaped

- plate on reduction in fluid forces acting on two tandem circular cylinders in a cross-flow", *J. Wind Eng. Ind. Aerod.*, **94**(7), 525-551. <https://doi.org/10.1016/j.jweia.2006.01.018>.
- Alam, M.M., Sakamoto, H. and Moriya, M. (2003), "Reduction of fluid forces acting on a single circular cylinder and two circular cylinders by using tripping rods", *J. Fluid. Struct.* **18**(3-4), 347-366. <https://doi.org/10.1016/j.jfluidstructs.2003.07.011>.
- Alam, M.M., Zhou, Y., Zhao, J.M., Flamand, O. and Buojuard, O. (2010), "Classification of the tripped cylinder wake and bi-stable phenomenon", *Int. J. Heat Fluid Fl.*, **31**(4), 545-560. <https://doi.org/10.1016/j.ijheatfluidflow.2010.02.018>.
- Alam, M.M., Elhimer, M., Longjun, W., Jacono, D.L. and Wong, C.W. (2018), "Vortex shedding from tandem cylinders", *Exp. Fluids*, **59-60**, 1-17.
- Bhatt, R., Maiti, D., Alam, M.M. and Rehman, S. (2018), "Couette-Poiseuille flow based on non-linear flow over a square cylinder near plane wall", *Wind Struct.*, **26**(5), 331-341. <https://doi.org/10.12989/was.2018.26.5.331>.
- Bhattacharyya, S. and Maiti, D.K. (2004), "Shear flow past a square cylinder near a wall", *Int. J. Eng. Sci.*, **42**(19-20), 2119-2134. <https://doi.org/10.1016/j.ijengsci.2004.04.007>.
- Chatterjee, D. and Mondal, C. (2012), "Forced convection heat transfer from tandem square cylinders for various spacing ratios", *Numer. Heat Transfer, Part A*, **61**(5), 381-400. <https://doi.org/10.1080/10407782.2012.647985>.
- Choi, S.U.S. (1995), "Enhancing thermal conductivity of fluid with nanoparticles in development and applications of non-newtonian flows", *ASME J. Heat Transf.*, **66**, 99-105.
- Devarakonda, R. and Humphrey, J.A.C. (1992), "Interactive computational-experimental methodologies in cooling of electronic components, Computer Mechanics Laboratory", Technical Report No.92-008, University of California, Berkeley.
- Eastman, J.A., Phillpot, S.R., Choi, S.U.S. and Keblinski, P. (2004), "Thermal transport in nanofluids", *Annu. Rev. Mater. Res.*, **34**, 219-246.
- Escher, W., Brunschweiler, T., Shalkevich, N., Shalkevich, A., Burgi, T., Michel, B. and Poulikakos, D. (2011), "On the cooling of electronics with nanofluids", *J. Heat Transf.*, **133**(5), 051401. doi:10.1115/1.4003283.
- Etmnan, A., Moosavi, M. and Ghaedsharafi, N. (2011), "Determination of flow configurations and fluid forces acting on two tandem square cylinders in cross flow and its wake pattern", *Int. J. Mechanics*, **5**, 63-74.
- Etmnan, F.V., Ebrahimnia, E., Niazmand, H. and Wongwises, S. (2012), "Unconfined laminar nanofluid flow and heat transfer around a square cylinder", *Int. J. Heat Mass Transfer*, **55**(5-6), 1475-1485. <https://doi.org/10.1016/j.ijheatmasstransfer.2011.10.030>.
- Haddad, Z., Abu-Nada, E., Hakan, F.O. and Mataoui, A. (2012), "Natural convection in nanofluids: Are the thermophoresis and Brownian motion effects significant in nanofluid heat transfer enhancement", *Int. J. Ther. Sci.*, **57**, 152-162. <https://doi.org/10.1016/j.ijthermalsci.2012.01.016>.
- Hwang, K.S., Lee, J.H. and Jang S.P. (2007), "Buoyancy-driven heat transfer of water-based Al_2O_3 nanofluids in a rectangular cavity", *Int. J. Heat Mass Transfer*, **50**(19-20), 4003-4010. <https://doi.org/10.1016/j.ijheatmasstransfer.2007.01.037>.
- Kim, S., Alam, M.M. and Maiti, D.K. (2018), "Wake and suppression of flow-induced vibration of a circular cylinder", *Ocean Eng.*, **151**, 298-307. <https://doi.org/10.1016/j.oceaneng.2018.01.043>.
- Kim, S., Alam, M.M. and Russel, M. (2016), "Aerodynamics of a cylinder in the wake of a V-shaped object", *Wind Struct.*, **23**(2), 143-155. <http://dx.doi.org/10.12989/was.2016.23.2.143>.
- Lee, S., Choi, S.U.S. and Li, S. and Eastman, J.A. (1999), "Measuring thermal conductivity of fluids containing oxide nanoparticles", *J. Heat Transfer*, **121**(2), 280-289. doi:10.1115/1.2825978.
- Leonard, B.P. (1979), "A stable and accurate convective modeling procedure based on quadratic upstream interpolation", *Comput. Method. Appl. M.*, **19**(1), 59-98. [https://doi.org/10.1016/0045-7825\(79\)90034-3](https://doi.org/10.1016/0045-7825(79)90034-3).
- Maiti, D.K. (2012), "Aerodynamic characteristics of rectangular cylinders near a wall", *Ocean Eng.*, **54**, 251-260.
- Maiti, D.K. and Bhatt, R. (2015), "Interactions of vortices of a square cylinder and a rectangular vortex generator under Couette-Poiseuille flow", *J. Fluid. Eng. T ASME*, **137**(5), 051203-051203-22. doi: 10.1115/1.4029631.
- Maiti, D.K., Bhatt, R. and Alam, M.M. (2016), "Aerodynamic forces on square cylinder due to secondary flow by rectangular vortex generator in offset tandem: comparison with Inline", *Comput. Fluids*, **134-135**, 157-176. <https://doi.org/10.1016/j.compfluid.2016.05.005>.
- Nguyen, C.T., Roy, G., Gauthier, C. and Galanis, N. (2007), "Heat transfer enhancement using Al_2O_3 -water nanofluid for an electronic liquid cooling system", *Appl. Thermal Eng.*, **27**(8-9), 1501-1506. <https://doi.org/10.1016/j.applthermaleng.2006.09.028>.
- Patankar, S.V. (1980), "Numerical heat transfer and fluid flow", Hemisphere Publishing Corporation, Taylor and Francis Group, New York.
- Sarkar, S. and Ganguly, S. (2012), "Analysis of entropy generation during mixed convective heat transfer of nanofluids past a square cylinder in vertically upward flow", *J. Heat Transfer*, **134**(12), 122501. doi:10.1115/1.4007411.
- Sarkar, S., Ganguly, S. and Biswas, G. (2012), "Mixed convective heat transfer of nanofluids past a circular cylinder in cross flow in unsteady regime", *Int. J. Heat Mass Transfer*, **55**(17-18), 4783-4799. <https://doi.org/10.1016/j.ijheatmasstransfer.2012.04.046>.
- Sarkar, S., Ganguly, S. and Dalal, A. (2013), "Buoyancy-driven flow and heat transfer of nanofluids past a square cylinder in vertically upward flow", *Int. J. Heat Mass Transfer*, **59**, 433-450. <https://doi.org/10.1016/j.ijheatmasstransfer.2012.12.032>.
- Sarkar, S., Ganguly, S., Biswas, G. and Saha, P. (2016), "Effect of cylinder rotation during mixed convective flow of nanofluids past a circular cylinder", *Comput. Fluids*, **127**, 47-64. <https://doi.org/10.1016/j.compfluid.2015.12.013>.
- Sarkar, S., Ganguly, S., Dalal, A., Saha, P. and Chakraborty, S. (2013), "Mixed convective flow stability of nanofluids past a square cylinder by dynamic mode decomposition", *Int. J. Heat Fluid Fl.*, **44**, 624-634. <https://doi.org/10.1016/j.ijheatfluidflow.2013.09.004>.
- Sharma, S., Maiti, D.K., Alam, M.M. and Sharma, B.K. (2018), "Nanofluid ($H_2O-Al_2O_3/CuO$) flow over a heated square cylinder near a wall under the incident of Couette flow", *J. Mech. Sci. Tech.*, **32**(2), 659-670.
- Shuja, S.Z., Yilbas, B.S. and Budair, M.O. (2001), "Vortex shedding over a rectangular cylinder with ground effect: flow and heat transfer characteristics", *Int. J. Heat Fluid Fl.*, **12**, 916-939.
- Sohankar, A. and Etmnan, A. (2009), "Forced-convection heat transfer from tandem square cylinders in cross flow at low Reynolds numbers", *Int. J. Numer. Meth. Fl.*, **60**(7), 733-751. <https://doi.org/10.1002/flid.1909>.
- Talebi, F., Houshang, A.M. and Shahi, M. (2010), "Numerical study of mixed convection flow in a square lid driven cavity utilizing nanofluids", *Int. J. Heat Mass Transfer*, **37**(1), 79-90. <https://doi.org/10.1016/j.icheatmasstransfer.2009.08.013>.
- Tatsutani, R., Devarakonda, R. and Humphrey, J.A.C. (1993), "Unsteady flow and heat transfer for cylinder pairs in a channel", *Int. J. Heat Mass Transfer*, **36**(13), 3311-3328. [https://doi.org/10.1016/0017-9310\(93\)90013-V](https://doi.org/10.1016/0017-9310(93)90013-V).
- Valipour, M.S. and Ghadi, A.Z. (2011), "Numerical investigation

- of fluid flow and heat transfer around a solid circular cylinder utilizing nanofluid”, *Int. Commun. Heat Mass Transfer*, **38**(9), 1296-1304. <https://doi.org/10.1016/j.icheatmasstransfer.2011.06.007>.
- Wang, Q. and Jaluria, Y. (2002), “Unsteady mixed convection in a horizontal channel with protruding heated blocks and a rectangular vortex promoter”, *Phys. Fluids*, **14**(7), 2113-2127. <https://doi.org/10.1063/1.1480832>.
- Yang, R.J. and Fu, L.M. (2001), “Thermal and flow analysis of a heated electronic component”, *Int. J. Heat Mass Transfer*, **44**(12), 2261-2275. [https://doi.org/10.1016/S0017-9310\(00\)00265-9](https://doi.org/10.1016/S0017-9310(00)00265-9).
- Yang, Y., Zhang, Z.G., Grulke, E.A., Anderson, W.B. and Wu, G. (2005), “Heat transfer properties of nanoparticle-in-fluid dispersions (nanofluids) in laminar flow”, *Int. J. Heat Mass Transfer*, **48**(6), 1107-1116. <https://doi.org/10.1016/j.ijheatmasstransfer.2004.09.038>.
- Zafar, F. and Alam, M.M. (2018), “A low Reynolds number flow and heat transfer topology of a cylinder in a wake”, *Phys. Fluids*, **30**(8), 083603. <https://doi.org/10.1063/1.5035105>.

